Acta Cryst B
STRUCTURAL SCIENCE
CRYSTAL ENGINEERING
MATERIALS
ISSN 2052-5206

Joint crystallization of $KCuAl[PO_4]_2$ and $K(Al,Zn)_2[(P,Si)O_4]_2$: crystal chemistry and mechanism of formation of phosphate-silicate epitaxial heterostructure

Olga Yakubovich,[a]* Galina Kiriukhina,[a,b] Larisa Shvanskaya,[a] Anatoliy Volkov[a,b] and Olga Dimitrova[a]

[a]M.V. Lomonosov Moscow State University, Leninskye Gory 1, Moscow, 119991, Russian Federation, and [b]The Institute of Experimental Mineralogy RAS, Akademika Osip'yana st 4, Chernogolovka, Moscow region 142432, Russian Federation. *Correspondence e-mail: yakubol@geol.msu.ru

Received 18 March 2020
Accepted 25 April 2020

Edited by J. Hadermann, University of Antwerp, Belgium

Keywords: X-ray diffraction; potassium copper aluminophosphate; phosphate-silicate heterostructure; coherent scattering; epitaxial oscillatory zoning; crystal chemistry; functional materials.

CCDC references: 1999127; 1999128

Supporting information: this article has supporting information at journals.iucr.org/b

Two novel phases, potassium copper aluminium bis(phosphate), $KCuAl[PO_4]_2$ (I), and potassium zinc aluminium bis(phosphate-silicate), $K(Al,Zn)_2[(P,Si)O_4]_2$ (II), were obtained in one hydrothermal synthesis experiment at 553 K. Their crystal structures have been studied using single-crystal X-ray diffraction. (I) is a new member of the $A^+M^{2+}M^{3+}[PO_4]_2$ family. Its open 3D framework built by AlO_5 and PO_4 polyhedra includes small channels populated by columns of CuO_6 octahedra sharing edges, and large channels where K^+ ions are deposited. It is assumed that the stability of this structure type is due to the pair substitution of Cu/Al with Ni/Fe, Co/Fe or Mg/Fe in different representatives of the series. From the $KCuAl[PO_4]_2$ structural features, one may suppose it is a potentially electrochemically active material and/or possible low-temperature antiferromagnet. In accordance with results obtained from X-ray diffraction data, using scanning electron microscopy, microprobe analysis and detailed crystal chemical observation, (II) is considered as a product of epitaxial intergrowth of phosphate $KAlZn[PO_4]_2$ and silicate $KAlSi[SiO_4]_2$ components having closely similar crystal structures. The assembly of 'coherent intergrowth' is described in the framework of a single diffraction pattern.

1. Introduction

The extensive present-day interest of the scientific community in the study of first-row transition metal phosphates is due to their physicochemical properties, the most important of which are magnetism and electrochemical activity. The promise of fluoro-phosphates and vanadates as magnetically and electrochemically active materials has been shown in recent research [see, for example, Keates *et al.* (2013)]. Novel materials based on phosphates with 2D and 1D subsystems of the magnetic structure, formed by first-row transition metals, show highly functional characteristics, inherent to frustration of the exchange interaction of magnetically active ions (Shvanskaya *et al.*, 2015; Yakubovich, Kiriukhina *et al.*, 2013; Yakubovich, Yakovleva *et al.*, 2013). Research into the physical properties of such objects lies in the field of quantum cooperative phenomena and contributes to the development of theoretical ideas about the structure of matter (Lin & Ding, 2013).

The operation of modern electric energy storage batteries is based on the ability of alkali metal ions to migrate inside the cathode material, *viz*. to penetrate the crystalline structure

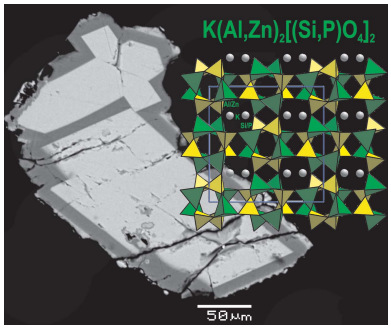

during a battery discharge and to be extracted during charging. Commercial usage of synthetic triphylite, $LiFePO_4$, as a cathode material with increased working voltage stimulated a new interest in mineral-like phosphates of alkali and transition metals. Particular attention is currently being paid to compounds with Na and K atoms due to their greater availability and lower cost, in comparison with Li (Kubota *et al.*, 2018; Pramudita *et al.*, 2017).

Recently, we have analysed the crystal chemical diversity of isoformula phosphates $AMM'[PO_4]_2$ (A^+ = Na, K, Rb, NH_4, M^{2+} = Cu, Ni, Co, Fe, Zn, M'^{3+} = Fe, Al, Ga), including 18 representatives (Yakubovich *et al.*, 2019). It has been shown that the rich crystal chemistry of the discussed morphotropic series (seven structure types) is due to the possibility of different coordination of M and M' atoms in the oxygen environment, from tetrahedral to octahedral, including five vertices, as well as to the size of alkali metal ions. It should be emphasized that some members of this family have a number of significant physical properties. Thus, $KCuFe[PO_4]_2$ is an antiferromagnet, also demonstrating the electrochemical properties of conductivity based on the migration of potassium ions through open channels of the crystal structure (Badri *et al.*, 2011).

Within a programme to explore the synthesis and crystal structures of compounds, potentially interesting as possible battery electrodes and/or magnetic materials, the phosphate crystallization system was complicated by the addition of the SiO_2 component in order to expand the chemical diversity of growing phases and to investigate crystal chemical regularities governing the formation of a particular structure. This article is aimed at providing the results of structural research of two new K/Al-bearing members of the $AMM'[TO_4]_2$ family, obtained in middle-temperature hydrothermal conditions.

2. Experimental: synthesis and crystallization

The title compounds were obtained in one trial of soft hydrothermal synthesis carried out in a 5 ml stainless steel bomb protected by a fluoroplastic coating. A starting mixture of $Al(OH)_3$, $K_4P_2O_7$, $Zn(NO_3)_2$, $CuCl_2$ and SiO_2 in a 3:3:3:1:1 weight ratio with distilled water filled 80% of the autoclave. The duration of the experiment at T = 553 K and P = 70 MPa was 14 days. The pH value of the crystallization medium measured after the experiment and cooling the autoclave was equal to 6. The obtained products were separated by filtration, washed with water, dried and analysed with a scanning electron microscope (Jeol JSM-6480LV Oxford X-Max^N) equipped with an energy-dispersive diffraction spectrometer (performed at the Laboratory of Local Methods for Studying Materials, Department of Petrology, Faculty of Geology, M. V. Lomonosov Moscow State University). Most of the trial (~80%) was represented by intergrowths of very small (up to 0.05 mm) flattened prismatic crystals of blue colour of various intensities. Crystals of the second phase, in much smaller quantities, are also very small light-green isometric individuals, as shown in Fig. 1.

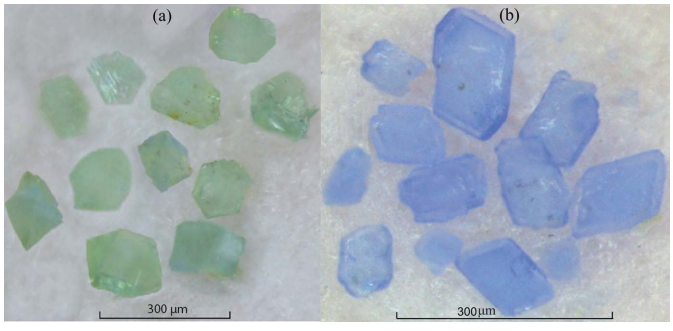

Figure 1
Photos of crystals of the title compounds: $KCuAl[PO_4]_2$ (*a*) and $K(Al,Zn)_2[(P,Si)O_4]_2$ (*b*).

According to the results of preliminary qualitative microprobe analysis, Cu, K, P, Al, O were present in the composition of the light-green crystals [hereafter (I)], while Zn, K, P, Al, Si, O were identified in the blue crystals [hereafter (II)]. To obtain quantitative data on the chemical composition the crystals were pressed into epoxy resin and the obtained polished carbon-coated samples were examined on the same microscope for composition using microprobe analysis at an accelerating voltage of 20 kV and a current of 10 nA. The electron beam flux was limited to 10 lumen to minimize sample destruction; spectrum accumulation time was 100 s. The following standards were used: anorthite, $CaAl_2Si_2O_8$, for determining Al and Si, synthetic $KTiPO_5$ for P, potassium feldspar, $KAlSi_3O_8$, for K, ZnS for Zn, and copper metal for Cu.

3. Results and discussion

Crystal data, data collection and structure refinement details are summarized in Table 1. All calculations were performed with *SHELX* programs (Sheldrick, 2015*a*,*b*) in the framework of the *WinGX* software package (Farrugia, 2012). The formulae $KCuAl[PO_4]_2$ (I) and $K(Al,Zn)_2[(P,Si)O_4]_2$ (II) correspond to established crystal structures and coincide well with chemical data. From the information obtained, it can be seen that the atoms of the *d* elements (Cu and Zn) were distributed between the phases during crystallization, and that the Si atoms became part of the blue crystals, exclusively. Presumably, there was a separation of the solution into regions of increased concentrations of Cu on the one hand and Zn and Si on the other. Two chemical reactions describing (I) and (II) formation may be supposed within the suggested paradigm:

$Al(OH)_3 + CuCl_2 + K_4P_2O_7 \Rightarrow KCuAl[PO_4]_2 + 2KCl + KOH + H_2O$;

$6Al(OH)_3 + 2Zn(NO_3)_2 + 3K_4P_2O_7 + 2SiO_2 \Rightarrow 2K_2Al_3ZnP_3SiO_{16} + 4KNO_3 + 4KOH + 7H_2O$.

3.1. Crystal structure of $KCuAl[PO_4]_2$ (I)

The average result of a quantitative microprobe analysis of phase (I) at two points is K_2O 14.86, CuO 24.42, Al_2O_3 15.8, P_2O_5 44.42, total 99.5 wt%. The formula of the compound calculated on the basis of four cations ($Cu^{2+} + Al^{3+} + 2P^{5+}$) is $K_{1.01}Cu_{0.99}Al_{1.00}P_{2.01}O_{8.02}$ and matches the formula

Table 1
Experimental details.

	(I)	(II)
Crystal data		
Chemical formula	$AlCuKO_8P_2$	$Al_3K_2O_{16}P_3SiZn$
M_r	319.56	601.51
Crystal system, space group	Monoclinic, $P2_1/c$	Monoclinic, $C2/c$
Temperature (K)	293	293
a, b, c (Å)	5.0270 (8), 14.047 (2), 9.263 (1)	13.234 (1), 13.121 (1), 8.6581 (8)
β (°)	102.29 (1)	100.14 (1)
V (Å^3)	639.11 (15)	1479.9 (2)
Z	4	4
Radiation type	Mo $K\alpha$	Mo $K\alpha$
μ (mm^{-1})	4.72	2.89
Crystal size (mm)	0.07 × 0.06 × 0.06	0.06 × 0.06 × 0.05
Data collection		
Diffractometer	Xcalibur, Sapphire3	Xcalibur, Sapphire3
Absorption correction	Multi-scan (*CrysAlis PRO*). Empirical absorption correction using spherical harmonics, implemented in *SCALE3 ABSPACK* scaling algorithm.	Gaussian (*CrysAlis PRO*). Numerical absorption correction based on Gaussian integration over a multifaceted crystal model.
T_{min}, T_{max}	0.957, 1.000	0.800, 0.856
No. of measured, independent and observed [$I > 2\sigma(I)$] reflections	9355, 1469, 1360	8821, 1303, 1176
R_{int}	0.057	0.060
(sin $\theta/\lambda)_{max}$ (Å^{-1})	0.650	0.594
Refinement		
$R[F^2 > 2\sigma(F^2)]$, $wR(F^2)$, S	0.049, 0.093, 1.23	0.059, 0.096, 1.29
No. of reflections	1469	1303
No. of parameters	122	118
Weighting scheme	$w = 1/[\sigma^2(F_o^2) + (0.014P)^2 + 5.5P]$ where $P = (F_o^2 + 2F_c^2)/3$	$w = 1/[\sigma^2(F_o^2) + (0.014P)^2 + 13.2P]$ where $P = (F_o^2 + 2F_c^2)/3$
$\Delta\rho_{max}$, $\Delta\rho_{min}$ (e Å^{-3})	0.63, −1.02	0.42, −0.42

Computer programs: *CrysAlis PRO* (version 1.171.37.35, release 13-08-2014 CrysAlis171.NET, compiled Aug. 13 2014,18:06:01) (Agilent, 2014), *SHELXT* (Sheldrick, 2015*a*,*b*), *SHELXL2016/6* (Sheldrick, 2015*a*,*b*), *DIAMOND* (Brandenburg, 2006).

$KCuAl[PO_4]_2$ established as a result of the X-ray diffraction study.

A symmetrically independent fragment of the structure of (I) includes a Cu-centred octahedron, an AlO_5 five-vertex polyhedron, two PO_4 tetrahedra and two K atoms (Fig. 2).

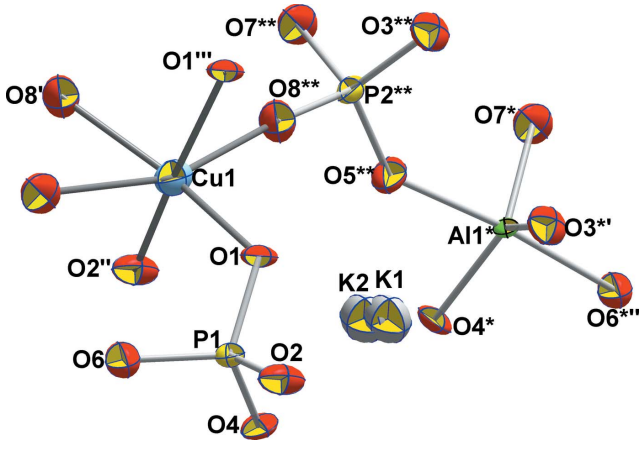

Figure 2
A view of $KCuAl[PO_4]_2$, showing the basic structural units with the atom-labelling scheme. Displacement ellipsoids are presented at the 90% probability level. Symmetry codes: (*) $1+x, \frac{3}{2}-y, \frac{1}{2}+z$; (**) $2-x, \frac{1}{2}+y, \frac{3}{2}-z$; (′) $x, \frac{3}{2}-y, -\frac{1}{2}+z$; (′′) $1+x, y, z$; (′′′) $1-x, 2-y, 1-z$; (*′) $x, \frac{5}{2}-y, \frac{1}{2}+z$; (*′′) $1+x, y, 1+z$.

Oxygen octahedra around Cu are characterized by four close Cu—O distances in the range 1.942 (4)–2.014 (4) Å, and two longer distances of 2.317 (4) and 2.431 (4) Å (Table 2). Such a distortion of the CuO_6 octahedra is typical of the Cu^{2+} ion of the d^9 configuration and is associated with the static Jahn–Teller effect. The Al—O bond lengths in AlO_5 trigonal bipyramids are split into two groups of close values. These are three distances in the interval 1.794 (4)–1.802 (4) Å, and two distances in *trans* positions equal to 1.885 (4) and 1.909 (4) Å. The P—O bond lengths in the P-centred tetrahedra range from 1.512 (4) to 1.558 (2) Å, with the same average value of 1.532 (4) Å. The distortion pattern of the Cu-, Al- and P-centred polyhedra is consistent with the bond valence data (Brown & Altermatt, 1985) (Table 3). Large K atoms split between two positions statistically populated 80% (K1) and 20% (K2) are surrounded by nine O atoms at distances in the interval 2.858 (7)–3.244 (9) Å, or by 11 O atoms, with K—O distances ranging from 2.75 (2) to 3.39 (2) Å.

Centrosymmetric four-membered rings built by AlO_5 and $P2O_4$ polyhedra sharing vertices form chains parallel to the [100] direction. Each of these chains at the vertices and centre of the unit cell is associated with four neighbouring chains through corner-bridging linkage provided by $P1O_4$ tetrahedra (Fig. 3) to assemble a 3D $[Al(PO_4)_2]^{3-}{}_\infty$ anionic *para*-framework. All oxygen vertices of the AlO_5 bipyramids are shared with P-centred tetrahedra, while two vertices of the

Table 2
Selected bond lengths (Å) for (I).

K1 and K2 represent an 80:20 split of the K site.

Cu1—O2^{i}	1.942 (4)	K2—O6^{v}	3.03 (2)
Cu1—O1	1.981 (4)	K2—O8^{iv}	3.07 (2)
Cu1—O8^{ii}	2.010 (4)	K2—O3^{v}	3.11 (2)
Cu1—O1^{iii}	2.014 (4)	K2—O5^{vii}	3.24 (3)
Cu1—O8^{iv}	2.317 (4)	K2—O6^{vi}	3.27 (3)
Cu1—O7^{ii}	2.431 (4)	K2—O2^{i}	3.29 (3)
K1—O4	2.858 (8)	K2—O7^{vii}	3.39 (2)
K1—O6^{v}	2.873 (7)	P1—O6	1.519 (4)
K1—O2^{vi}	2.887 (6)	P1—O2	1.527 (4)
K1—O5^{vii}	2.893 (14)	P1—O4	1.530 (4)
K1—O3^{v}	2.894 (9)	P1—O1	1.558 (4)
K1—O1	2.935 (7)	P2—O5	1.512 (4)
K1—O5^{iv}	3.110 (7)	P2—O8	1.525 (4)
K1—O4^{v}	3.189 (14)	P2—O3	1.529 (4)
K1—O7^{vii}	3.219 (8)	P2—O7	1.543 (4)
K1—O8^{iv}	3.244 (9)	Al1—O7	1.794 (4)
K2—O4	2.75 (2)	Al1—O4	1.800 (4)
K2—O1	2.85 (2)	Al1—O3^{viii}	1.802 (4)
K2—O2^{vi}	2.886 (19)	Al1—O6^{v}	1.884 (4)
K2—O5^{iv}	3.02 (2)	Al1—O5^{ix}	1.908 (4)

Symmetry codes: (i) $x+1, y, z$; (ii) $x, -y+\frac{3}{2}, z-\frac{1}{2}$; (iii) $-x+1, -y+2, -z+1$; (iv) $-x+2, y+\frac{1}{2}, -z+\frac{3}{2}$; (v) $x, -y+\frac{3}{2}, z+\frac{1}{2}$; (vi) $x+1, -y+\frac{3}{2}, z+\frac{1}{2}$; (vii) $-x+1, y+\frac{1}{2}, -z+\frac{3}{2}$; (viii) $x-1, y, z$; (ix) $-x+1, -y+1, -z+1$.

Table 3
Bond valence data for $KCuAl[PO_4]_2$.

The calculation is made without considering the splitting of the K position.

Atom	K	Cu	Al	P1	P2	Σ
O1	0.114	0.442		1.173		2.13
		0.404				
O2	0.130	0.491		1.275		1.90
O3	0.127		0.665		1.268	2.06
O4	0.141		0.668	1.265		2.13
	0.057					
O5	0.128		0.498		1.328	2.03
	0.071					
O6	0.135		0.531	1.303		1.97
O7	0.053	0.131	0.679		1.221	2.08
O8	0.050	0.409			1.282	1.92
		0.178				
Σ	1.00	2.05	3.04	5.02	5.10	

$P1O_4$ and one vertex of the $P2O_4$ tetrahedra remain 'pendant', *e.g.* not shared with other polyhedra of the aluminophosphate framework. Columns of the CuO_6 octahedra sharing edges are included in an open space between 'pendant' vertices of the PO_4 tetrahedra. Owing to the distortion of phosphate tetrahedra, as well as to the valence contributions of K and Cu atoms, a local bond balance at the corresponding oxygen atoms is achieved (Table 3). The large K atoms are placed in open framework channels restricted by six-membered windows.

$KCuAl[PO_4]_2$ crystallizes in a structure type established for phosphates of the $AM^{2+}M^{3+}[PO_4]_2$ (A = K, Rb; M^{2+} = Ni, Mg, Co, Cu; M^{3+} = Fe, Al) family (Yakubovich *et al.*, 2019 and references therein), obtained by the flux method and in hydrothermal conditions. The new compound is the second in this row, along with $RbCuAl(PO_4)_2$, containing Cu as the divalent metal and Al as the trivalent metal. A feature of their crystal structures, in comparison with the structures of Ni, Co or Mg ferriphosphates, is the CuO_6 octahedra distortion with four close Cu—O distances in the Cu-centred squares and two substantially removed apical O atoms in the *trans* position. As a second dissimilarity, we note significantly smaller sizes of AlO_5 bipyramids with an average Al—O distance of 1.838 (4) Å compared with the sizes of FeO_5 polyhedra, for which the average Fe—O distances are 1.93–1.94 Å. Such differences in geometry allow us to conclude that this structure type is quite stable, since it is realized upon the occupancy of $M^{3+}O_5$ polyhedra by either Al^{3+} cations or significantly larger Fe^{3+} cations. Moreover, simultaneous replacement of the relatively regular $M^{2+}O_6$ (M^{2+} = Ni, Mg, Co) octahedra by strongly distorted CuO_6 polyhedra, in accordance with the Jahn–Teller effect, also occurs in the framework of the same 3D configuration. It is very likely that the stability of this structure type is due just to the pair substitution of Cu/Al with Ni/Fe, Co/Fe or Mg/Fe. It is also important to emphasize that isotype phases with alkali metal atoms of both K and Rb may be realized for copper aluminium phosphates, *i.e.* the $ACuAl[PO_4]_2$ crystal structure is stable with changing alkali metal atom in the channels of the heteropolyhedral frame-

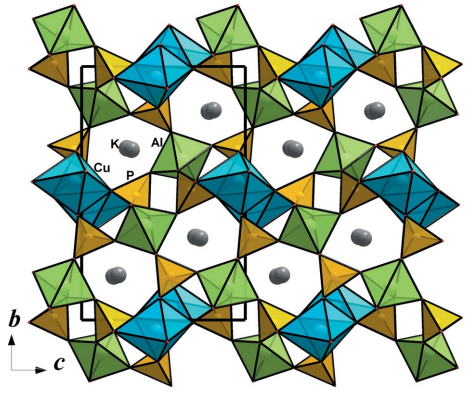

Figure 3
The $KCuAl[PO_4]_2$ crystal structure displayed along the *a* axis.

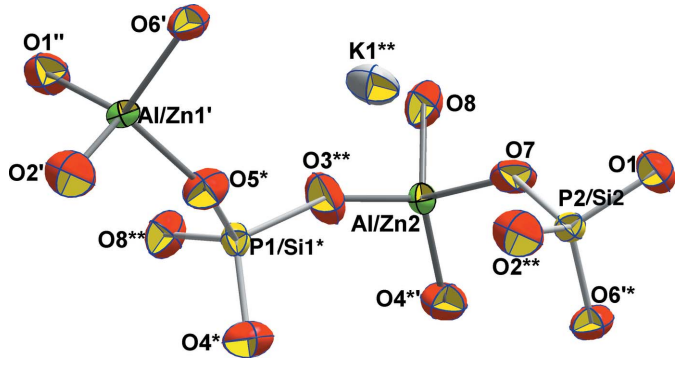

Figure 4
Basic structural units for $K(Al,Zn)_2[(P,Si)O_4]_2$ with the atom-labelling scheme. Displacement ellipsoids are presented at the 70% probability level. Symmetry codes: (*) $x, y, -1+z$; (**) $x, 1-y, -\frac{1}{2}+z$; (′) $\frac{1}{2}-x, -\frac{1}{2}+y, -\frac{1}{2}-z$; (″) $\frac{1}{2}-x, \frac{1}{2}+y, -\frac{1}{2}-z$; (*′) $1-x, y, \frac{1}{2}-z$; (′*) $1-x, 1-y, -z$.

work. In addition, the displacement of K atoms from the centre of the channels and their occupation of two structural positions at unacceptably short distances suggest the possibility of migration of the alkaline cations through the crystal structure and allow prediction of the associated ion-exchange, ion-conducting and/or electrochemical properties of the mineralogically probable aluminophosphate.

A study of the magnetic behaviour of the Rb analogue, $RbCuAl(PO_4)_2$, showed that at T_N = 10.5 K the compound orders antiferromagnetically and exhibits spontaneous magnetization (Yakubovich *et al.*, 2016). Similar magnetic properties can be expected for the K species.

3.2. Crystal structure of $K(Al,Zn)_2[(P,Si)O_4]_2$ (II)

The main structural units that form the $K(Al,Zn)_2[(P,Si)O_4]_2$ crystal structure present two pairs of symmetrically independent tetrahedra and large K atoms. Refined close amounts of atoms in two independent positions jointly populated by Al^{3+} and Zn^{2+} ions [G_{Al1} = 0.749 (5) and G_{Al2} = 0.738 (5)] were fixed at the values of 0.75 for the final refinement. Thus, two $(Al,Zn)O_4$ tetrahedra are mainly occupied by Al, and two $(P,Si)O_4$ tetrahedra by P atoms (Fig. 4). The tetrahedra of the first type centred by Al and Zn, statistically distributed in a ratio of ∼3:1, are similar in size and distortion; the Al/Zn—O distances lie in the range 1.754 (4)–1.796 (4) Å, and the average Al/Zn—O distances in the tetrahedra are 1.778 (4) and 1.771 (4) Å and practically equal (with an accuracy of the standard deviation) (Table 4). These values are obviously larger than the average Al—O distance, 1.747 Å, for the AlO_4 tetrahedra in the ordered structure of anorthite, $CaAl_2Si_2O_8$ (Wainwright & Starkey, 1971), and significantly smaller than the average Zn—O distance, 1.940 Å, for the Zn atom in tetrahedral coordination (Yakubovich & Melnikov, 1989), which is consistent with a significant prevalence of Al in these polyhedra.

Table 4
Selected bond lengths (Å) for (II).

Al1—O2	1.760 (5)	P2—O7	1.543 (5)
Al1—O1^{i}	1.769 (5)	P2—O2^{iii}	1.545 (5)
Al1—O5^{ii}	1.785 (4)	P2—O6^{vi}	1.549 (4)
Al1—O6	1.796 (4)	K1—O7^{ii}	2.749 (4)
Al2—O3^{iii}	1.753 (5)	K1—O5^{ii}	2.880 (5)
Al2—O4^{iv}	1.771 (5)	K1—O6^{vii}	2.974 (4)
Al2—O8	1.774 (5)	K1—O4^{ii}	2.983 (5)
Al2—O7	1.785 (5)	K1—O3	3.000 (5)
P1—O3^{v}	1.539 (5)	K1—O5^{iii}	3.017 (5)
P1—O5	1.546 (4)	K1—O1^{ii}	3.104 (5)
P1—O8^{v}	1.550 (5)	K1—O2	3.114 (5)
P1—O4	1.555 (5)	K1—O8^{ii}	3.194 (5)
P2—O1	1.541 (5)	K1—O7^{v}	3.366 (5)

Symmetry codes: (i) $x, y+1, z$; (ii) $-x+\frac{1}{2}, y+\frac{1}{2}, -z+\frac{1}{2}$; (iii) $x, -y+1, z-\frac{1}{2}$; (iv) $-x+1, y, -z+\frac{1}{2}$; (v) $x, -y+1, z+\frac{1}{2}$; (vi) $-x+1, -y+1, -z$; (vii) $-x+\frac{1}{2}, -y+\frac{3}{2}, -z$.

An amount of P and Si in both independent positions (∼3:1) was set based on a requirement of the electroneutrality of the chemical formula, because the P:Si ratio cannot be refined using X-ray diffraction data due to the similar scattering power of these atoms. The bond lengths in both symmetrically independent $(P,Si)O_4$ tetrahedra vary in close limits with the average (P,Si)—O distances equal to 1.547 (4) and 1.544 (4) Å, which confirms the similar distribution of phosphorus and silicon atoms over two structural positions. These values show a major amount of P atoms in polyhedra, since usual average P—O distances for orthophosphates are equal to 1.530 Å (Yakubovich & Urusov, 1997), whereas the average Si—O distances are 1.614 Å (Wainwright & Starkey, 1971). The K atoms are at the centre of nine-vertex polyhedra with K—O distances ranging from 2.746 (4) to 3.196 (4) Å; the tenth O atom is located 3.367 (5) Å away from the K site.

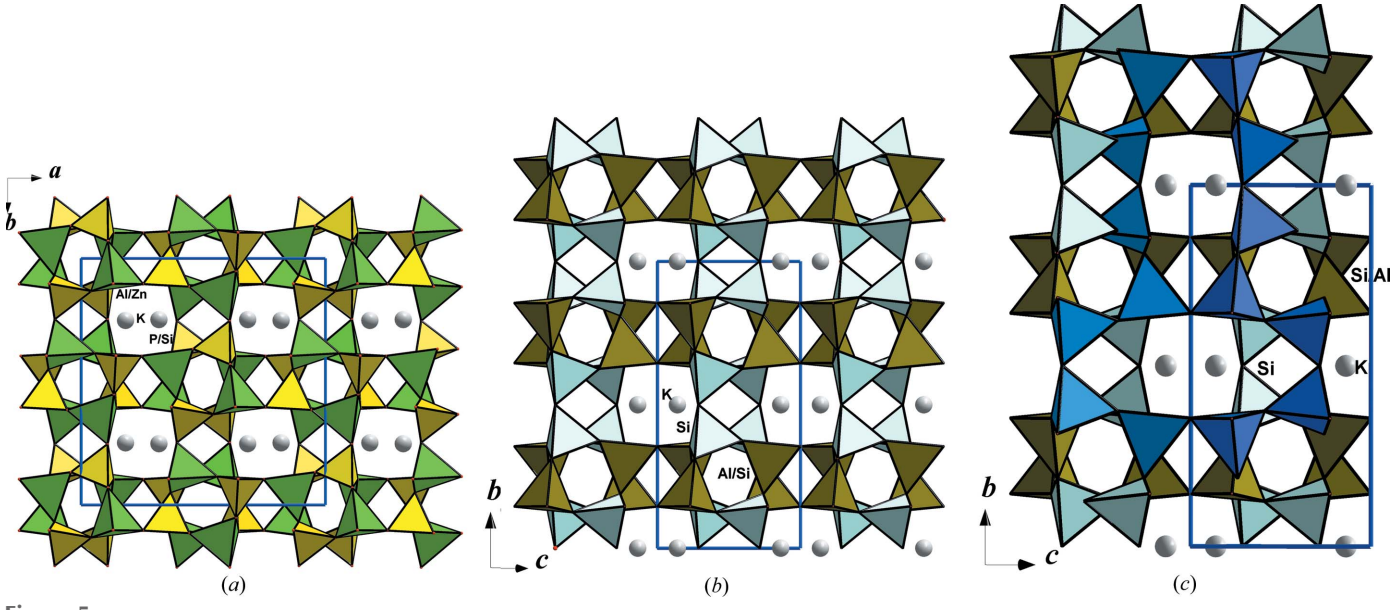

Figure 5
The crystal structures of $K(Al,Zn)_2[(P,Si)O_4]_2$ (*a*) and $K(Al,Si)_2[SiO_4]_2$ (*b*) viewed along an axis of about 8.6 Å. The eight-membered rings built by $[(Al,Si)O_4]$ and $[SiO_4]$ tetrahedra sharing vertices in $K(Al,Si)_2[SiO_4]_2$, of the same topology as in the $K(Al,Zn)_2[(P,Si)O_4]_2$ structure, are shown in dark blue (*c*).

The crystal structure of $K(Al_{1.5}Zn_{0.5})[(P_{1.5}Si_{0.5})O_8]$ is a 3D network of two types of tetrahedra, statistically populated by two different atoms. In the first case, these are Al and Zn metal atoms, in the second P atoms (non-metal, typical acid-forming agent) and Si (metalloid). A mixed-type anionic framework built from alternating $(Al,Zn)O_4$ and $(P,Si)O_4$ tetrahedra sharing vertices is stabilized by large K^+ ions in the cavities [Fig. 5(*a*)]. The minerals celsian, $BaAl_2Si_2O_8$ (Griffen & Ribbe, 1976), and filatovite, $K(Al,Zn)_2[(As,Si)O_4]_2$ (Filatov *et al.*, 2004), crystallize in the same structure type, as do a large group of phosphates with first-row transition metals and Al (Yakubovich *et al.*, 2019). The structural feature of the isotypic natural and synthetic compounds of this family is the close topology of their cationic substructures to that of feldspars with the characteristic design of a 'crosslinked Jacob's ladder' (Taylor, 1933) (Fig. 6).

3.3. Composite $K(Al,Zn)_2[(P,Si)O_4]_2$ crystals as a product of epitaxial intergrowth of $KAlSi[SiO_4]_2$ and $KAlZn[PO_4]_2$

The above data show the coincidence of the chemical compositions of the $K(Al,Zn)_2[(P,Si)O_4]_2$ phase, obtained by microprobe analysis and as a result of the crystal structure refinement. At the same time, it is known that crystal structures with isomorphic occupancy of positions in oxygen tetrahedra by P and Si atoms are quite rare, among synthetic compounds and minerals. Most often, if these elements together are part of the mineral composition, they are distributed at different positions, for example, in the crystal structures of phosinaite (Krutik *et al.*, 1980; McDonald *et al.*, 1996), harrisonite (Grice & Roberts, 1993) or lomonosovite (Belov *et al.*, 1977). Bearing this in mind, an additional study of phase (II) was undertaken using a scanning electron microscope. An obvious separation of the crystals into two zones with sharply defined regions differing in colour was observed (Fig. 7).

To obtain quantitative data on the chemical composition of both stuck fragments, a microprobe analysis of polished crystals of $K(Al,Zn)_2[(P,Si)O_4]_2$, at two points of the light and two points of the dark sectors, was undertaken. It revealed a clear correlation between the colour of the studied areas and their chemical composition. Thus, P and Zn atoms on one hand and Si atoms on the other hand occur distributed between sectors with different colours. The average chemical composition of the light part of the sample was found to be 'phosphate': K_2O 14.91, ZnO 24.22, Al_2O_3 17.04, P_2O_5 45.20, total 101.37 wt%, while the average chemical composition of the dark part is essentially 'silicate': K_2O 11.33, ZnO 1.14, Al_2O_3 13.82, P_2O_5 3.81, SiO_2 68.18, total 98.28 wt%. The empirical formulae corresponding to these two compositions, calculated for four cations that form the framework of the crystal structure, are as follows: $K_{0.99}Zn_{0.95}Al_{1.05}P_{2.00}O_{8.02}$ and $K_{0.65}Zn_{0.04}Al_{0.74}P_{0.15}Si_{3.08}O_{7.99}$. The idealized formulae are $KZnAlP_2O_8$ and $KAlSi_3O_8$.

When dealing with microbeam analysis it is difficult to avoid capturing a neighbouring region in a double-phase crystal, with diverse composition of its components. A comparison of the sizes of the light and dark areas of the studied samples has allowed us to assume partial 'capture' of neighbouring light fragments of phosphate composition, when the electronic probe is exposed to narrow areas of dark coloration (see Fig. 7). Despite the measures taken (limiting the diameter of the electron beam), such an effect may happen. It is shown by small amounts of P and Zn atoms in the results of chemical analysis of the silicate section.

The observed configuration (Fig. 7), with a high probability, represents the epitaxial intergrowth of two phases of different composition: zincaluminophosphate, $K(Zn,Al)_2[PO_4]_2$, and aluminosilicate, $KAlSi_3O_8$. The photograph clearly shows a large zone of the light areas of the phosphate composition within the crystals, in comparison with the smaller size of the dark areas of silicate. This observation correlates with the initial amounts of the corresponding reagents used in the crystal synthesis. A significantly larger volume of the phosphate component in the solution apparently caused the primary nucleation and growth of the phosphate crystal. Gradually, as P and Zn were scooped up by the growing crystal and depleted locally, when a threshold concentration of Si was reached on the surface of the phosphate crystal, the formation

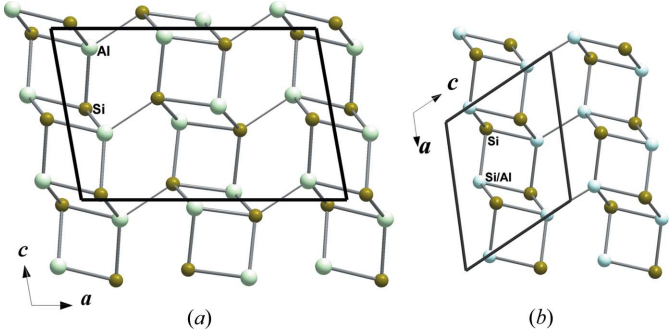

Figure 6
The cationic arrangements formed by 'Jacob's ladder' chains of atom-centred tetrahedra in the celsian (*a*) and orthoclase (feldspar) (*b*) structures.

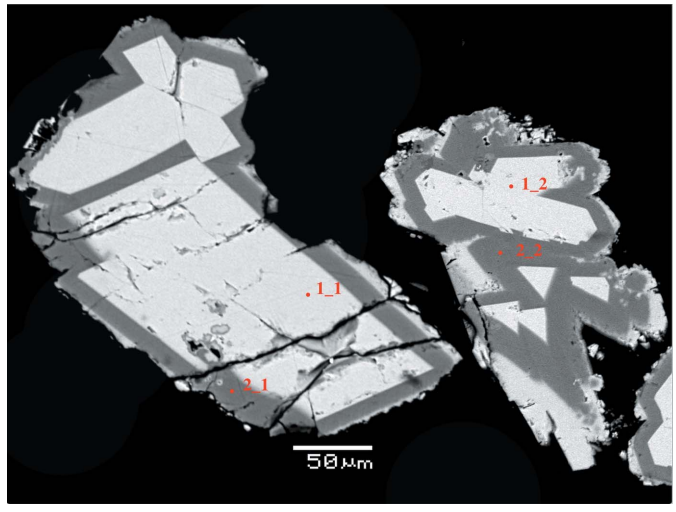

Figure 7
Polished zoned crystals (II) of epitaxial intergrowth of silicate (dark) and phosphate (light) components. Scanning electron microscopy image, backscattered-electron mode.

Table 5
Crystal data for the group of $K(M,M')_2[TO_4]_2$ compounds with mixed anionic frameworks built from tetrahedra.

Ionic radii of cations in tetrahedral surrounding of the O atoms: $R_{Al}^{3+} = 0.51$, $R_{Zn}^{2+} = 0.74$, $R_{Si}^{4+} = 0.37$, $R_{P}^{5+} = 0.35$ Å.

Compound, structure type	Unit-cell parameters and volume [a, b, c (Å), β (°), V (Å^3)]	Space group, Z, ρ_c (g cm^{-3})	Distance limits M—O and T—O (Å)	Reference
$K^M(Al_{0.75}Zn_{0.25})_2{}^T[(P_{0.75}Si_{0.25})O_4]_2$ Celsian structure type: $BaAl_2[SiO_4]_2$	13.2340 (10), 13.1210 (10), 8.6581 (8), 100.140 (10), 1479.9 (2)	$C2/c$, 8, 2.700	1.754 (4)–1.796 (4), 1.537 (4)–1.555 (4)	This work
Orthoclase, $K^M(Al_{0.5}Si_{0.5})_2{}^T[SiO_4]_2$	8.5632 (11), 12.963 (14), 7.2099 (11), 116.073 (9), 718.9 (2) → $a' = d1 = 13.395$, $b = 12.963$, $c' = d2 = 8.427$, $\beta' = 100.89$, $V' = 1436.9$	$C2/m$, 4, 2.570	1.661 (5)–1.673 (5), 1.609 (5)–1.629 (5)	Prince *et al.* (1973)
$K^M(Al_{0.5}Zn_{0.5})_2{}^T[PO_4]_2$, Celsian structure type: $BaAl_2[SiO_4]_2$	13.2906 (7),13.1956 (8), 8.6660 (5), 99.920 (2), 1497.10 (5)	$C2/c$, 8, 2.852	1.814 (2)–1.852 (2), 1.514 (2)–1.531 (2)	Wang *et al.* (2020)

of silicate followed. During the development, a silicate crystal (the dark zone in Fig. 7) shielded the surface of the growth of the phosphate phase from the nutrient medium, until the Si concentration in it decreased to critical values at which point phosphate began to grow again, as shown by the light outer rim. Such zoning (rhythmic formations) during the growth of mineral aggregates is widespread in nature (Parsons *et al.*, 2015). Epitaxial oscillatory zoning, as a special case, is due to structural control. For instance, two sets of oscillatory zones developed during epitaxial growth of the mineral erythrite, $(Co,Zn,Ni,Fe)_3(AsO_4)_2{\cdot}8H_2O$, with inhomogeneous distributions of metal atoms in the octahedra, have been shown recently (Antao & Dhaliwal, 2017). Under the condition of geometric proportionality of crystallizing fragments, which is usually associated with the closeness of their crystal structures and is the basis for a continuous transition at the interface, the assemblies of 'coherent intergrowth' are realized, which can be described in the framework of a single diffraction pattern. Diffraction arises here as a single phenomenon because of the consistency of the phases of the scattered waves.

As noted above, a large group of first-row transition metal and/or aluminium phosphates with the general formula $AMM'[PO_4]_2$ crystallizes in the celsian, $BaAl_2Si_2O_8$, structure type. The isotypic celsian and filatovite, $K(Al,Zn)_2(As,Si)_2O_8$, are structurally similar to feldspar $KAlSi_3O_8$ (Prince *et al.*, 1973; Smith & Brown, 1988 and references therein) (Fig. 5), one of the most widespread minerals in the earth's crust. The crystal structure of the recently studied phosphate, $K(Zn,Al)_2[PO_4]_2$ (Wang *et al.*, 2020), with chemical composition being about 75% of the composition of the title epitaxial crystals $K(Al,Zn)_2[(P,Si)O_4]_2$ (Fig. 5), is also described by the celsian structure type. Crystal characteristics and cation–oxygen bond lengths in tetrahedra-forming structures of orthoclase, $K(Al_{0.5}Si_{0.5})_2[SiO_4]_2$, epitaxial intergrowth $K(Al_{0.75}Zn_{0.25})_2[(P_{0.75}Si_{0.25})O_4]_2$ and the phosphate phase $K(Al_{0.5}Zn_{0.5})_2[PO_4]_2$, are summarized in Table 5. From the presented data, a correlation is observed between the number of cations in the tetrahedra, the values of their ionic radii, and the sizes of unit cells of the compounds.

The crystal structures of the above minerals and synthetic phosphates are based on the topologically identical 2D networks with four- and eight-membered rings formed by two types of tetrahedra (Fig. 5). Such grid layers are combined into a framework by vertex-bridging of tetrahedra adjacent along the third crystallographic axis. Large K atoms are placed in the framework channels. The mentioned analogy is characteristic not only for layers, but also in the rotation of tetrahedra relative to the net planes. 3D constructions of tetrahedra in both cases can be interpreted as assembled from eight-membered rings of two types: *UUUUDDDD* and *UDDU-DUUD*, where the symbols *U* and *D* denote the directions of

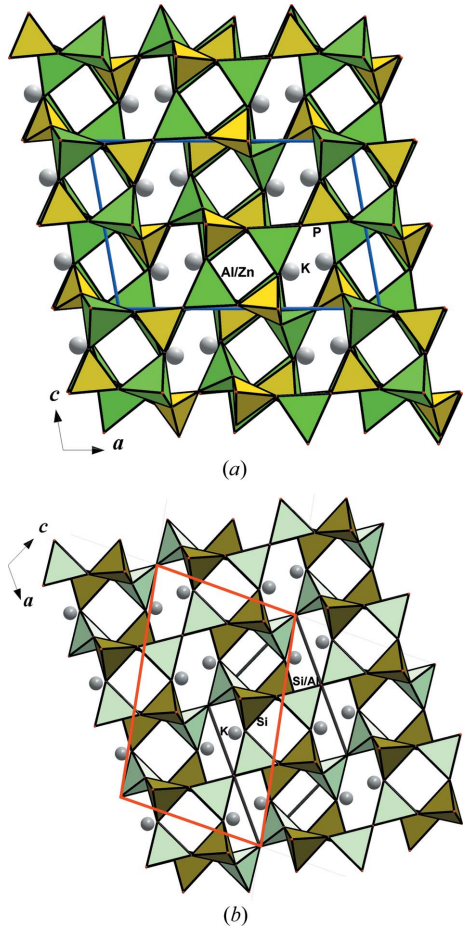

Figure 8
The crystal structures of $K(Al_{0.5}Zn_{0.5})_2[PO_4]_2$ (celsian structure type) (*a*) and orthoclase $K(Al_{0.5}Si_{0.5})_2[SiO_4]_2$ (*b*) projected along the monoclinic axis. The diagonals of the orthoclase *ac* plane (Table 5) are shown in red.

the apical vertices of the tetrahedra (up and down) relative to the plane of the layer.

From the information available (Wang *et al.*, 2020), the activation energies for electrical transport were found to be equal to 0.49 eV for $K(Zn,Al)_2(PO_4)_2$. It means that potassium ions are ready to migrate through structure channels at increasing temperature under an external electric field. Similar behaviour of the K ions can be expected in the case of epitaxial phosphate-silicate crystals.

The difference in the sizes of unit cells of the two discussed structure types, as can be seen in Fig. 5, is associated with the different population of polyhedra in the eight-membered rings (Brown & Parsons, 1989). Thus, in the orthoclase, $K(Al_{0.5}Si_{0.5})_2[SiO_4]_2$, structure there are alternating pairs of one type of tetrahedron within the rings (Si-Si-Al/Si-Al/Si-Si-Si-Al/Si-Al/Si . . .), while in the $K(Al_{0.5}Zn_{0.5})_2[PO_4]_2$ (and celsian) structure different tetrahedra alternate through one (P-Al/Zn-P-Al/Zn-P-Al/Zn-P-Al/Zn . . .) ring. This situation leads to an almost twofold increase in one of the unit-cell parameters of the phosphate phase in comparison with the size of the same period in the isoformula silicate analogue, and to nearly a doubling in the unit-cell volume of the latter (Table 5). Likewise, an alternative distribution of cations in the tetrahedra of eight-membered rings correlates with a change of the symmetry group from $C2/m$, characterizing the $K(Al_{0.5}Si_{0.5})_2[SiO_4]_2$ crystal structure, to $C2/c$ in the structure of $K(Al_{0.5}Zn_{0.5})_2[PO_4]_2$. It is noteworthy that these two monoclinic space groups are coupled by the group–subgroup relation.

The similarity of the silicate and phosphate structures is also revealed in the xz projection (Fig. 8). The close unit-cell parameters along the monoclinic axes (∼13 Å) and the comparable sizes of the other two parameters (a and c) of $K(Al_{0.5}Zn_{0.5})_2[PO_4]_2$ with the sizes of the diagonals of the xz plane of $K(Al_{0.5}Si_{0.5})_2[SiO_4]_2$ (Table 5) emphasize their structural similarity and topological correspondence.

In accordance with the condition of geometric proportionality of crystallizing fragments, which is associated with the proximity of the structures of the two phases and is the basis for a continuous transition at the interface, a 'coherent intergrowth' structure is formed, which can be described in the framework of a single diffraction pattern (Fig. 9). Indeed, coherent intergrowth along grain boundaries of two components different in chemical composition but close in crystal structure ensures the diffraction pattern of a single-phase sample. Since in the X-ray diffraction experiment we collect information on the averaged crystal structure and make calculations based on the intensities of reflections obtained from such a mixed crystal, the resulting crystal chemical formula $K(Al_{0.75}Zn_{0.25})_2[(P_{0.75}Si_{0.25})O_4]_2$ corresponds to the quantitative ratios of the two phases in the composition of the sample with an 'epitaxial heterostructure', for which an X-ray diffraction study was performed.

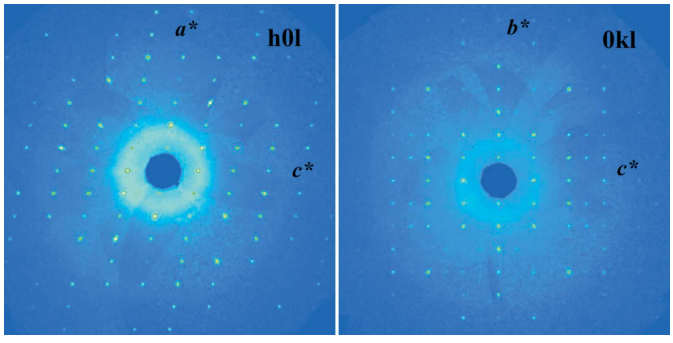

Figure 9
Diffuse reflections, marking small incoherency on the phase boundary of the phosphate and silicate components, on the $h0l$ and $0kl$ layers of the reciprocal lattice of the epitaxial phosphate-silicate heterocrystal.

In a recent paper (Shchipalkina *et al.*, 2020) a continuous solid–solution between potassium feldspar $KAlSi_3O_8$ and filatovite $K(Al,Zn)_2(As,Si)_2O_8$ from Tolbachik fumaroles was discussed. The authors pointed out that a slow transition from K feldspar to filatovite, due to increasing the As_2O_5 content from the central part to the peripheral zones of a crystal, can be occasionally observed within one sample. Based on numerous microprobe analyses, they concluded that the substitution scheme $Al^{3+} + As^{5+} \rightarrow 2Si^{4+}$, which controls the conversion of K feldspar to filatovite, should be expanded with a more complex equation, *e.g.* $M^{2+} + As^{5+} \rightarrow Al^{3+} + Si^{4+}$, where M^{2+} corresponds to Zn and Cu. This assumption allowed proposition of the formula of a Si-free end-member of filatovite, $KAlZnAs_2O_8$. Curiously, this hypothetical arsenate with celsian structure type exactly corresponds to the phosphate component $KAlZnP_2O_8$ of our epitaxial composite.

4. Conclusion

Two novel phases $KCuAl(PO_4)_2$ (I) and $K(Al,Zn)_2[(P,Si)O_4]_2$ (II) were obtained in one hydrothermal synthesis experiment. We assume that the phase formation process started from the separation of Cu and Zn atoms between two phases, and Si atoms entering into only one of them. (I) and (II) were investigated using scanning electron microscopy, microprobe analysis and X-ray diffraction. (I) crystallizes in the $KNiFe[PO_4]_2$ structure type inherent for the first subgroup of the $AM^{2+}M^{3+}(PO_4)_2$ family (A = K, Rb; M^{2+} = Ni, Mg, Co, Cu; M^{3+} = Fe, Al). We have supposed that the stability of this structure type is due to the pair substitution of Cu/Al with Ni/Fe, Co/Fe or Mg/Fe. Based on crystal chemical features of (I) we consider the compound as a potential candidate for an electrochemically active material and/or a possible low-temperature antiferromagnet.

In accordance with obtained experimental data and detailed crystal chemical analysis of (II) we came to the conclusion that composite $K(Al,Zn)_2[(P,Si)O_4]_2$ crystals present the product of an epitaxial intergrowth of the silicate $KAlSi[SiO_4]_2$ and phosphate $KAlZn[PO_4]_2$ phases with identical topology of their cationic substructures and similar crystal structures (that of the minerals orthoclase and celsian, accordingly). Our assumption was based on the results of a morphological study of the samples with a clear division into two zones with sharply defined boundaries and strongly different colours. A microprobe analysis of light and dark sectors revealed their differing

compositions, *e.g.* phosphate and silicate. In our opinion, the two-phase crystal studied using X-ray diffraction was the assembly of phosphate and silicate 'coherent intergrowth' with epitaxial 'heterostructure', which could be described in the framework of a single diffraction pattern due to phase matching of scattered waves. The proposed scenario is supported by rare cases of isomorphic distribution of P and Si atoms in oxygen tetrahedra in crystal structures of mineral and synthetic solids. Most often, if these elements together are part of one crystal, they occupy different structural positions.

Acknowledgements

We are much obliged to N. G. Zinovieva and I. V. Pekov for a fruitful discussion and valuable comments. We thank N. N. Koshlyakova for the microprobe analysis of the crystals. We are also grateful to N. V. Zubkova for her help with the X-ray experiments.

Funding information

The following funding is acknowledged: Russian Foundation for Basic Research (grant No. 18-29-12076 to Olga Yakubovich); Russian Science Foundation (grant No. 19-77-00081 to Galina Kiriukhina).

References

Agilent (2014). *CrysAlis PRO*. Agilent Technologies Ltd, Yarnton, Oxfordshire, England.
Antao, S. M. & Dhaliwal, I. (2017). *Minerals*, **7**, 136.
Badri, A., Hidouri, M., López, M. L., Pico, C., Wattiaux, A. & Amara, M. B. (2011). *J. Solid State Chem.* **184**, 937–944.
Belov, N. V., Gavrilova, G. S., Solov'eva, L. P. & Khalilov, A. D. (1977). *Sov. Phys. Dokl.* **22**, 422–424.
Brandenburg, K. (2006). *DIAMOND*. Crystal Impact GbR, Bonn, Germany.
Brown, I. D. & Altermatt, D. (1985). *Acta Cryst.* B**41**, 244–247.
Brown, W. L. & Parsons, I. (1989). *Mineral. Mag.* **53**, 25–42.
Farrugia, L. J. (2012). *J. Appl. Cryst.* **45**, 849–854.
Filatov, S. K., Krivovichev, S. V., Burns, P. C. & Vergasova, L. P. (2004). *Eur. J. Mineral.* **16**, 537–543.
Grice, J. D. & Roberts, A. C. (1993). *Can. Mineral.* **31**, 781–785.
Griffen, D. T. & Ribbe, P. H. (1976). *Am. Mineral.* **61**, 414–418.
Keates, A. C., Armstrong, J. A. & Weller, M. T. (2013). *Dalton Trans.* **42**, 10715–10724.
Krutik, V. M., Pushcharovskii, D. Yu., Khomyakov, A. P., Pobedimskaya, E. A. & Belov, N. V. (1980). *Sov. Phys. Crystallogr.* **26**, 679–682.
Kubota, K., Dahbi, M., Hosaka, T., Kumakura, Sh. & Komaba, Sh. (2018). *Chem. Rec.* **18**, 459–479.
Lin, R. & Ding, Y. (2013). *Materials*, **6**, 217–243.
McDonald, A. M., Chao, G. Y. & Grice, J. D. (1996). *Can. Mineral.* **34**, 107–114.
Parsons, I., Fitz Gerald, J. D. & Lee, M. R. (2015). *Am. Mineral.* **100**, 1277–1303.
Pramudita, J. C., Sehrawat, D., Goonetilleke, D. & Sharma, N. (2017). *Adv. Energy Mater.* **7**, 1602911.
Prince, E., Donnay, G. & Martin, R. F. (1973). *Am. Mineral.* **58**, 500–507.
Shchipalkina, N. V., Pekov, I. V., Britvin, S. N., Koshlyakova, N. N. & Sidorov, E. G. (2020). *Phys. Chem. Miner.* **47**, 1–15.
Sheldrick, G. M. (2015*a*). *Acta Cryst.* A**71**, 3–8.
Sheldrick, G. M. (2015*b*). *Acta Cryst.* C**71**, 3–8.
Shvanskaya, L., Yakubovich, O., Bychkov, A., Shcherbakov, V., Golovanov, A., Zvereva, E., Volkova, O. & Vasiliev, A. (2015). *J. Solid State Chem.* **222**, 44–52.
Smith, J. V. & Brown, W. L. (1988). *Feldspar Minerals.* 1. *Crystal Structures, Physical, Chemical and Microstructural Properties.* Berlin, Heidelberg, New York, London, Paris, Tokyo: Springer-Verlag.
Taylor, W. H. (1933). *Z. Kristallogr.* **85**, 425–442.
Wainwright, J. E. & Starkey, J. (1971). *Z. Kristallogr.* **133**, 75–84.
Wang, H., Geng, L., Wang, Y.-J., Lu, H.-Y. & Meng, Ch.-Y. (2020). *J. Alloys Compd.* **820**, 153176.
Yakubovich, O., Kiriukhina, G., Dimitrova, O., Volkov, A., Golovanov, A., Volkova, O., Zvereva, E., Baidya, S., Saha-Dasgupta, T. & Vasiliev, A. (2013). *Dalton Trans.* **42**, 14718–14725.
Yakubovich, O., Kiriukhina, G., Volkov, A. & Dimitrova, O. (2019). *Acta Cryst.* C**75**, 514–522.
Yakubovich, O. V., Kiriukhina, G. V., Dimitrova, O. V., Zvereva, E. A., Shvanskaya, L. V., Volkova, O. S. & Vasiliev, A. N. (2016). *Dalton Trans.* **45**, 2598–2604.
Yakubovich, O. V. & Melnikov, O. K. (1989). *Kristallografiya*, **34**, 62–66.
Yakubovich, O. V. & Urusov, V. S. (1997). *Crystallogr. Rep.* **42**, 261–268.
Yakubovich, O. V., Yakovleva, E. V., Golovanov, A. N., Volkov, A. S., Volkova, O. S., Zvereva, E. A., Dimitrova, O. V. & Vasiliev, A. N. (2013). *Inorg. Chem.* **52**, 1538–1543.